Distinct Viscoelasticity of Nanoparticle-Tethering Polymers Revealed by Nonequilibrium Molecular Dynamics Simulations

Pengxiang Xu, Jiaping Lin,* and Liangshun Zhang*

Shanghai Key Laboratory of Advanced Polymeric Materials, State Key Laboratory of Bioreactor Engineering, Key Laboratory for Ultrafine Materials of Ministry of Education, School of Materials Science and Engineering, East China University of Science and Technology, Shanghai 200237, China

S Supporting Information

ABSTRACT: We employed nonequilibrium molecular dynamics simulations to study viscoelastic properties of nanoparticle-tethering polymers. Effects of nanoparticle−polymer interaction and molecular architecture on the viscoelasticity are investigated. The results show that the nanoparticle-tethering polymers with attractive nanoparticle−polymer interaction exhibit enhanced storage and loss moduli relative to the homopolymers or bare nanoparticle/polymer blend. In addition, the storage and loss moduli of nanoparticle-tethering polymers can be further enhanced through tuning their molecular architectures, such as increasing the nanoparticle diameter or decreasing the polymer chain length. From the physical origin, the enhancement of dynamic moduli originates from the slowdown of polymer dynamics, which arises from the attractive nanoparticle−polymer interaction, the tethering covalent bond, and the obstacle of nanoparticles. The present work not only reveals the physical origin of distinct viscoelasticity of nanoparticle-tethering polymers, but also provides useful information for preparing advanced materials based on these organic/inorganic components.
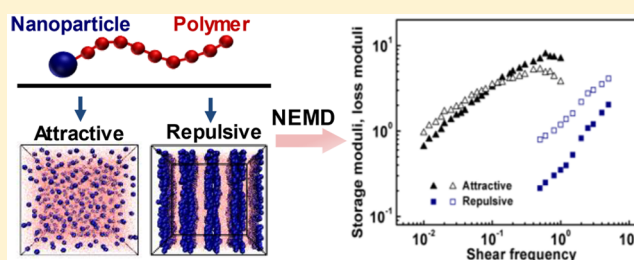
1. INTRODUCTION

Embedding inorganic nanoparticles (NPs) into polymer matrices can improve the mechanical, thermal, optical, and rheological properties of polymer materials due to the synergistic effect between the NPs and the polymer matrices.[1−4] These organic/inorganic hybrid materials may find potential applications in semiconductor, electronic devices, and biomedical products.[5−7] The organic/inorganic composites generally exhibit distinct viscoelastic properties because the organic component provides toughness and the inorganic one provides stiffness. Hence, the investigation on the viscoelasticity of this type of material is essential both in theoretical research and engineering applications. However, the immiscibility between the organic polymers and the inorganic NPs generally results in the aggregation of NPs, which may adversely affect the viscoelasticity. Some chemical or physical modifications are performed to eliminate this adverse effect. Tethering the NPs with the polymer chains via covalent bonds is an effective approach. It prevents the aggregation of NPs through the sterical stabilization by surrounding polymers.[8−12]

Recently, many types of NPs have been used to tether with polymer chains and form NPs-tethering polymers (NTPs), such as C_{60}-poly(methyl methacrylate),[13] silica-polystyrene,[14,15] Fe_3O_4-polystyrene,[16] polyhedral oligomeric silsesquioxane-polystyrene,[17,18] and C_{60}-polystyrene.[19] In these NTPs, NPs are well dispersed in the polymer matrices or self-assemble into various anisotropic microstructures, such as strings and connected sheets.[20−25] Much effort has been devoted to investigate the viscoelasticity of NTPs.[26−31] It was revealed that tethering NPs with polymer chains not only increases the NP dispersion but also enhances the dynamic moduli, that is, storage (G') and loss (G'') moduli. For instance, Genix and coauthors studied the linear rheology of silica NPs grafted by styrene butadiene rubber.[26] As the grafting density increases, the average aggregation degree of silica NPs decreases, leading to the enhancement of terminal dynamic moduli and the increase of relaxation times. Kumar's group investigated the mechanical properties of silica-tethering polystyrene (PS) dispersed in PS matrices.[30] In this hybrid material, the ductility of glassy PS matrices substantially increases, while the elastic moduli and the yield stress maintain. In spite of these studies, the physical origin of enhanced viscoelasticity in the NTP system is still not understood. Moreover, the dynamics of polymers in NTPs, which is different from that of free polymer chains, is not clear in experiments.

Apart from the experiments, theoretical simulation methods, such as dissipative particle dynamics,[32,33] polymer reference interaction site model,[34] and molecular dynamics (MD)[35−43] are useful tools to investigate the viscoelasticity and the dynamics of NTPs. For example, equilibrium molecular dynamics (EMD) is utilized to study the viscoelasticity of polymer matrices embedding NPs.[38] It is found that the

enhancement of dynamic moduli originates from additional distortion of shear field and slower relaxation dynamics of tethered chains compared to the matrix chains. Similarly, the effect of NPs on the relaxation behaviors of polymer chains was also confirmed by the EMD simulations in Kröger's group.[44,45] However, in the EMD, the conformation and the relaxation dynamics of polymer chains at nonequilibrium state cannot be monitored. Escobedo and coauthors performed nonequilibrium molecular dynamics (NEMD) simulations to investigate the steady-state shear properties of NTPs.[46] They found that the shear-induced increase of chain alignment can lead to the reduction of viscosity. Chen et al. adopted NEMD simulations to explore the strain amplitude-dependence viscoelasticity (i.e., Payne effect) of polymer/NPs composites.[47] They found that the Payne effect strongly depends on the NP–polymer interaction and the NP loading. In our previous work, we also employed the NEMD method to investigate the mechanical properties of NTPs.[48] It was found that the NTPs exhibit enhanced tensile modulus relative to the pure polymers and the bare NPs/polymer blends, which arises from the increases in bond orientation, bond stretching, and nonbonding interaction. Despite these studies on the steady-state behaviors, it is still necessary to study the oscillatory viscoelasticity of NTPs. Many important issues, such as the physical origin of distinct viscoelasticity as well as the relaxation dynamics of tethered polymers and NPs, remain to be studied. The success of NEMD simulations makes it ready to be extended to explore the polymer dynamics and predict the viscoelasticity of NTPs.

In this work, we present for the first time the NEMD simulations of oscillatory viscoelasticity of NTPs. The effects of NP–polymer interaction, polymer chain length, and NP diameter on the viscoelasticity of NTPs were examined. It was observed that the dynamic moduli of polymeric melts are enhanced by tethering the NPs with the end of the polymer chains, and the enhancement of dynamic moduli becomes more remarkable with increasing the strength of NP–polymer interaction, the NP diameter or decreasing the polymer chain length. To reveal the physical origin of the enhancement of dynamic moduli, mean square distances of various motion units (i.e., NPs, polymer chains, and single polymer beads) are monitored. This study could provide useful information to understand the relaxation dynamics of NPs and polymers as well as the relationship between the viscoelasticity and the microstructure of NTPs.

2. METHODS AND MODEL

2.1. Coarse-Grained Molecular Dynamics Method.

In the present work, we constructed a coarse-grained model of NTPs, as illustrated in Figure 1a. In this model, a polymer bead represents a cluster of atoms, consisting of numbers of repeat units.[49−51] Each polymer chain is mimicked as a linear bead–spring chain containing L beads with diameter σ. Every nanoparticle is represented by a Lennard-Jones (LJ) sphere with diameter d and tethered with a polymer chain via covalent bond. Thus, the tethered density of NPs is given by $1/\pi d^2$. To ensure the same density of each component, masses of polymer beads and NPs are set as m and $(d/\sigma)^3 m$, respectively.

In the MD method, the potentials consist of nonbonding potential U_{ij} and bonding potential U_{bond}. The nonbonding potential U_{ij} is given by the modified LJ 12:6 potential acting between any pair of ith and jth beads[52]
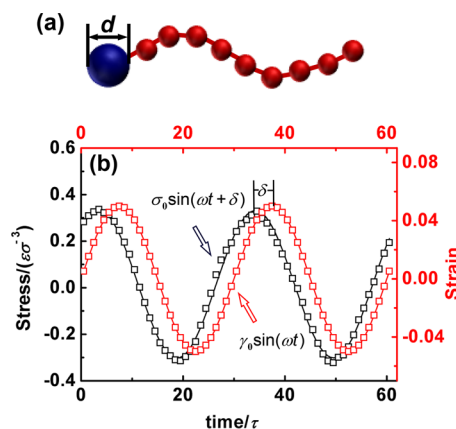

Figure 1. (a) Coarse-grained model of NPs-tethering polymer. The polymer chain is tethered onto the NP with diameter d. The blue and red beads represent the NP and polymer beads, respectively. (b) Typical curves of stress and strain as a function of time for NPs-tethering polymers. The strain amplitude and shear frequency are $\gamma_0 = 0.05$ and $\omega = 0.2\tau^{-1}$, respectively. The strain is given in advance and the stress calculated by eq 5 is in response to the applied strain. The solid lines are the sinusoidal fitted curves.

$$
U_{ij} = \begin{cases} 4\varepsilon_{ij}\left[\left(\dfrac{\sigma}{r_{ij}-r_{EV}}\right)^{12} - \left(\dfrac{\sigma}{r_{ij}-r_{EV}}\right)^{6} - \left(\dfrac{\sigma}{r_{ij}^{c}}\right)^{12} \right. \\ \left. \qquad + \left(\dfrac{\sigma}{r_{ij}^{c}}\right)^{6}\right], \qquad\qquad r_{ij}-r_{EV} \le r_{ij}^{c} \\ \\ 0, \qquad\qquad\qquad\qquad\qquad r_{ij}-r_{EV} > r_{ij}^{c} \end{cases} \quad (1)
$$

where ε_{ij} is the interaction strength, and r_{ij}^c is the cutoff distance. To account for the excluded volume effect, the interaction range is offset by r_{EV}, whose values of NP–NP, NP–polymer, and polymer–polymer are, respectively, set as $d-\sigma$, $(d-\sigma)/2$, and 0. The cutoff distance r_{ij}^c determines whether the interaction between the ith and jth beads is attractive ($r_{ij}^c > 2^{1/6}\sigma$) or repulsive ($r_{ij}^c \le 2^{1/6}\sigma$). In the present work, the interactions are truncated at an attractive cutoff distance ($r_{P-P}^c = 2.5\sigma$) for the polymer–polymer interaction and a repulsive cutoff distance ($r_{N-N}^c = 2^{1/6}\sigma$) for the NP–NP interaction.[48] The strengths of polymer–polymer interaction ε_{P-P} and the NP–NP interaction ε_{N-N} are fixed at ε. To simulate the systems having different NP–polymer interaction modes (i.e., attractive, repulsive, and neutral) and strengths, r_{N-P}^c and ε_{N-P} for the NP–polymer interaction are variable.

The bonding potential U_{bond} is given by the modified finite extensible nonlinear elastic (FENE) potential[53]

$$
U_{bond} = -0.5kR_0^2 \ln\left[1 - \left(\frac{r-r_{EV}}{R_0}\right)^2\right] \quad (2)
$$

where k and R_0 are, respectively, the elastic coefficient and the maximum extensible bond length. k and R_0 are set as $30\varepsilon/\sigma^2$ and 1.5σ to avoid unphysical bond crossing.[48]

In the MD simulations, reduced units are adopted for all physical quantities.[54] The units of mass, length, and energy are defined by m, σ, and ε, respectively. The time unit τ is defined as $\tau = (m\sigma^2/\varepsilon)^{1/2}$, and its real value can be estimated by matching the simulated lateral diffusion coefficient to the experimentally measured value.[54]

2.2. Nonequilibrium Simulation. Nonequilibrium simulation based on the standard MD method is employed to simulate the polymeric systems subjected to an oscillatory shear field. Lees-Edwards "sliding brick" boundary conditions were the most widely adopted to introduce a shear field.[55,56] Alternatively, we employ a "box deforming" technique which is conceptually identical to the Lees-Edwards boundary conditions.[47,57] In the simulations, SLLOD algorithm coupled with the "box deforming" technique is adopted to introduce a shear field in x-direction and velocity gradient in y-direction

$$\frac{d\mathbf{r}_i}{dt} = \mathbf{v}_i + \mathbf{e}_x \dot{\gamma} r_{i,y}$$

$$m_i \frac{d\mathbf{v}_i}{dt} = \mathbf{f}_i - m_i \mathbf{e}_x \dot{\gamma} v_{i,y} \tag{3}$$

where $\mathbf{e}_x$ is the unit vector along x-direction. $\mathbf{r}_i$, $\mathbf{v}_i$, and $\mathbf{f}_i$ are the position, velocity, and force of ith bead, respectively. $r_{i,y}$ and $v_{i,y}$ are the magnitudes of corresponding vector, where the subscript y denotes the y-component of vector. $\dot{\gamma}$ is the shear rate, which is the time derivative of shear strain γ. In the present work, the shear strain γ is given as a sinusoidal function $\gamma_0 \sin(\omega t)$, where γ_0 and ω are respectively the strain amplitude and the shear frequency. Thereby, the shear rate $\dot{\gamma}$ is a cosine function $\omega\gamma_0 \cos(\omega t)$. For a viscoelastic fluid under oscillatory shear, the stress in the shear plane is also a sinusoidal function, $\sigma_{xy} = \sigma_0 \sin(\omega t + \delta)$, where the phase angle δ is between $0°$ and $90°$. This sinusoidal function can be decomposed as $\sigma_{xy} = G' \sin(\omega t) + G'' \cos(\omega t)$, where G' is the storage (in-phase) modulus and G'' is the loss (out-phase) modulus

$$G' = \frac{\sigma_0}{\gamma_0} \cos(\delta), \quad G'' = \frac{\sigma_0}{\gamma_0} \sin(\delta) \tag{4}$$

In the nonequilibrium simulation, the σ_0 and δ are calculated through the sinusoidal curve fitting (see Figure 1b) of shear stress σ_{xy}

$$\sigma = \frac{1}{V} \left\langle \sum_i M_i \mathbf{v}_i \mathbf{v}_i + \frac{1}{2} \sum_{i \neq j} \mathbf{r}_{ij} \mathbf{F}_{ij} \right\rangle \tag{5}$$

Here, V denotes the volume of simulation box and the angular bracket represents ensemble average.

2.3. Model and Condition. We constructed a series of NTPs designated as $P_L N$-d, where P and N denote the polymer beads and the NPs, respectively. For instance, the NTP with chain length $L = 24$ and NP diameter $d = 2\sigma$ is denoted as $P_{24}N$-2. To generate an initial configuration, a large system with low NTP volume fraction ϕ_{NTP} was constructed in a cubic box of $100 \times 100 \times 100\sigma^3$ and then compressed to the ϕ_{NTP} of 0.45 (note that the size of NPs is not changed in the compression process). Herein, the ϕ_{NTP} is defined as the ratio of the volume of particles (including NPs and polymer beads) to the volume of box. For systems with different molecular architectures, the edge lengths of the compressed box were tuned to maintain the fixed NTP volume fraction of $\phi_{NTP} = 0.45$. For example, the edge lengths of box were set as 22.7σ for the system containing 315 $P_{24}N$-2 chains. After the construction of initial configurations, standard EMD simulations were performed in NPT ensemble by using the Nose-Hoover barostat and thermostat. Velocity-Verlet algorithm was adopted for 5×10^7 MD steps to achieve an equilibrium state with time step of $\Delta t = 0.004\tau$. To explore the oscillatory viscoelasticity, NEMD simulations were subsequently performed by transforming the cubic box to a triclinic one.[57] To check the finite size effect, the simulations with larger box size were conducted, such as a sample having 558 $P_{24}N$-2 chains in the box with edge lengths of 27.4σ. It is found that the simulations with different box sizes produce similar structures and viscoelastic properties. All of the simulations were carried out by using the large atomic/molecular massively parallel simulator (LAMMPS) developed by Sandia National Laboratory.[58]

3. RESULTS AND DISCUSSION

In this work, we focused on the linear viscoelasticity of NPs-tethering polymers $P_L N$-d. First, we investigated the viscoelasticity of representative NTP system and compared it with cases of homopolymer and bare NPs/polymer blend. Then, the effect of NP−polymer interaction on the viscoelasticity of NTP systems was examined. Last, the molecular architecture parameters, such as the NP diameter d and the polymer chain length L, were tuned to regulate the viscoelasticity of NTPs.

3.1. Enhanced Viscoelasticity of NPs-Tethering Polymers. In this subsection, we focused on the linear viscoelasticity of $P_{24}N$-2 system with attractive NP−polymer interaction. The corresponding cutoff distance r_{N-P}^c and strength ε_{N-P} were set as 2.5σ and 5.0ε, respectively. As a comparison, a model of homopolymer P_{24} was also constructed where the r_{P-P}^c and ε_{P-P} were the same as those in the $P_{24}N$-2 system (i.e., $r_{P-P}^c = 2.5\sigma$ and $\varepsilon_{P-P} = 1.0\varepsilon$).

It is well-known that the dynamic moduli of NPs-filled polymer composites under oscillatory shear depend on the strain amplitude γ_0 and the shear frequency ω. The dependence of dynamic moduli on strain amplitude, which is known as the Payne effect,[59−61] should be examined to ensure that the systems are in the linear viscoelastic regime. Figure 2a shows
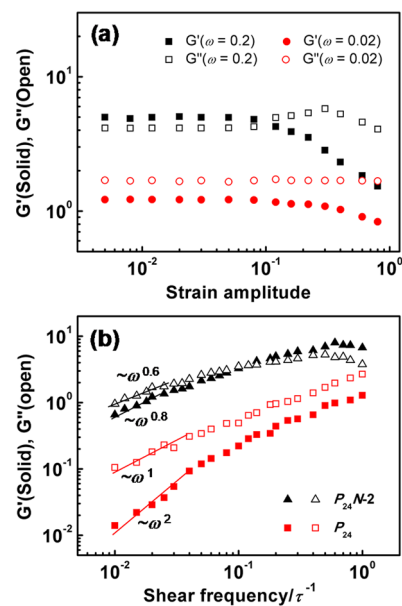

Figure 2. (a) Storage (G') and loss (G'') moduli as a function of strain amplitude for the $P_{24}N$-2 system under shear frequency of $\omega = 0.2\tau^{-1}$ and $\omega = 0.02\tau^{-1}$. (b) G' and G'' as a function of shear frequency for the NPs-tethering polymers $P_{24}N$-2 and the homopolymers P_{24}. The solid lines in the plot are the fitted curves of data obtained in the low regime of shear frequency from $0.01\tau^{-1}$ to $0.06\tau^{-1}$.

the strain-dependent storage modulus (G') and loss modulus (G'') of $P_{24}N$-2 system under shear frequencies of $\omega = 0.2\tau^{-1}$ and $\omega = 0.02\ \tau^{-1}$. The flow behaviors display two distinct regimes: strain-independent linear regime at small strain amplitudes and strain-dependent nonlinear regime at large strain amplitudes. In the regime of small strain amplitude, the shear flow is not strong enough to disturb the equilibrium structures, leading to the platform of G' and G''. In the regime of large strain amplitude, G' gradually decreases with increasing strain amplitude while G'' exhibits a pronounced maximum value, which originates from the structural breaking and the increase of energy dissipation. From the strain amplitude sweeps of G' and G'' (Figure 2a), it is clearly demonstrated that the NTPs exhibit the Payne effect. To ensure the linear viscoelastic behaviors, the strain amplitude is fixed at $\gamma_0 = 0.05$ within the linear regime in the following simulations.

Figure 2b shows the curves of G' and G'' versus shear frequency ω for the $P_{24}N$-2 NTPs and the P_{24} homopolymers. The measured range of ω is $0.01-1\tau^{-1}$. The data at lower frequencies are not shown because the statistic errors of stress are too large in lower frequency regime due to the strong thermal fluctuations. It can be seen from Figure 2b that both G' and G'' of $P_{24}N$-2 system are larger than those of P_{24} system, suggesting that the NTPs exhibit enhanced viscoelasticity compared to the homopolymers. The P_{24} system exhibits liquid-like viscoelasticity (i.e., $G' < G''$) with the terminal behavior of $G' \sim \omega^2$ and $G'' \sim \omega^1$.[62] For the $P_{24}N$-2 system, however, a crossover is observed in the curves of G' and G'' versus ω, indicating that a liquid-to-solid transition takes place with increasing shear frequency. Below the transition point ($\omega_c \approx 0.1\tau^{-1}$), G' is smaller than G'', and the power law indexes of G' and G'' plots in the low frequency regime are respectively 0.8 and 0.6, which are less than those for the P_{24} system. The relationships, $G' \sim \omega^{0.8}$ and $G'' \sim \omega^{0.6}$, deviate the terminal behaviors predicted by the Rouse model,[62] originating from the slowdown of polymer relaxation via the incorporation of tethered NPs. Above the transition point, the $P_{24}N$-2 system shows solid-like viscoelasticity (i.e., $G' > G''$). As the ω exceeds $0.6\tau^{-1}$, G'' decreases with increasing ω, while G' approaches a platform modulus G_N. Although the platform modulus of P_{24} system is absent within the measured range, it can be estimated as $G_N = \rho k_B T / N_P = 0.85\sigma\varepsilon^{-3}$, where ρ and N_P are, respectively, the density and the amount of polymer bead.[62] The platform modulus of $P_{24}N$-2 system ($7.2\sigma\varepsilon^{-3}$) is much larger than the estimated G_N of P_{24} system, further indicating that the NTPs can enhance the viscoelasticity of polymers.

The viscoelasticity of bare NPs/polymer blends was also examined to verify the enhancement of viscoelasticity of NTPs. A blend system, where the molecular architecture and the bead−bead interaction are the same as those in the $P_{24}N$-2 system, was constructed. The frequency sweeps of G' and G'' for both cases are shown in Figure S1a of Supporting Information (SI). It can be seen that the blend system also exhibits liquid-like viscoelasticity ($G' < G''$) in the low frequency regime and solid-like viscoelasticity ($G' > G''$) in the high frequency regime. The existence of transition point (marked by the arrows) is also clarified by the curve of loss factor $\tan \delta$ versus shear frequency ω shown in Figure S1b of SI. Compared to the blend system, G' of $P_{24}N$-2 system increases in the low frequency regime while G'' maintains invariable, but the transition point shifts to a lower frequency (from $0.2\tau^{-1}$ to $0.1\tau^{-1}$). These observations manifest the fact that tethering NPs with the end of polymers enhances the

elastic properties while maintains the flow properties compared to the bare NPs/polymer blends.

To get deeper insight into the physical origin of enhanced viscoelasticity of NTPs, the dynamics of NPs and polymers was examined. In the simulations, we monitor the motions of various basic units including NPs, polymer beads, and polymer chains. The dynamic properties of these motion units are estimated by the diffusion coefficients of NPs (D_N), polymer beads (D_P), and center-of-mass of polymer chains (D_{cm}). The diffusion coefficients are related to the mean square displacements (MSDs) of corresponding motion units[63]

$$D_k \propto \frac{1}{6} \lim_{t \to \infty} \frac{d}{dt} \mathrm{MSD}_k$$

$$\mathrm{MSD}_k = \langle [\mathrm{R}_k(t) - \mathrm{R}_k(0)]^2 \rangle \tag{6}$$

where D_k and $\mathbf{R}_k(t)$ are, respectively, the diffusion coefficient and the position of corresponding motion unit at time t. The angular bracket represents ensemble average. Figure 3a,b show the MSDs as a function of simulation time for the $P_{24}N$-2 system and the P_{24} system, respectively. The motion units in both systems exhibit diffusive behaviors (i.e., the MSDs increase linearly with time), which are used to estimate the diffusion coefficients. For the $P_{24}N$-2 system, the D_{cm}, D_N, and D_P have
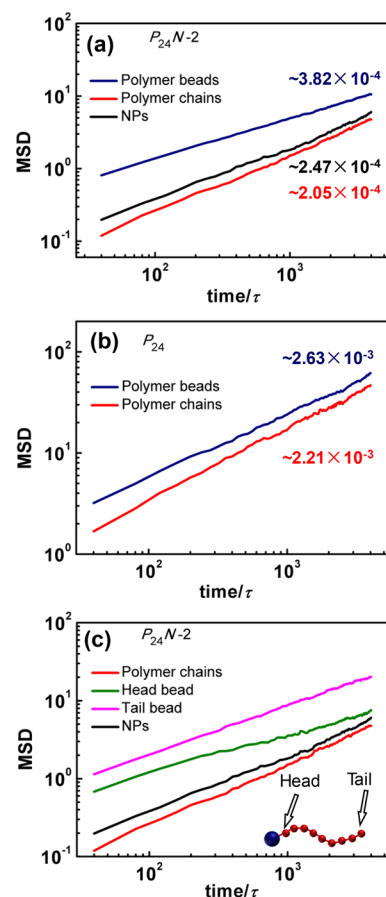

Figure 3. Mean square displacements (MSDs) of polymer beads (blue), NPs (black), and center-of-mass of polymer chains (red) as a function of simulation time for (a) the $P_{24}N$-2 system and (b) the P_{24} system. The diffusion coefficients are highlighted in the plots. (c) MSDs of the head and tail beads, center-of-mass of polymer chains, and NPs as a function of time for the $P_{24}N$-2 system. The inset shows the definitions of the head and tail beads.
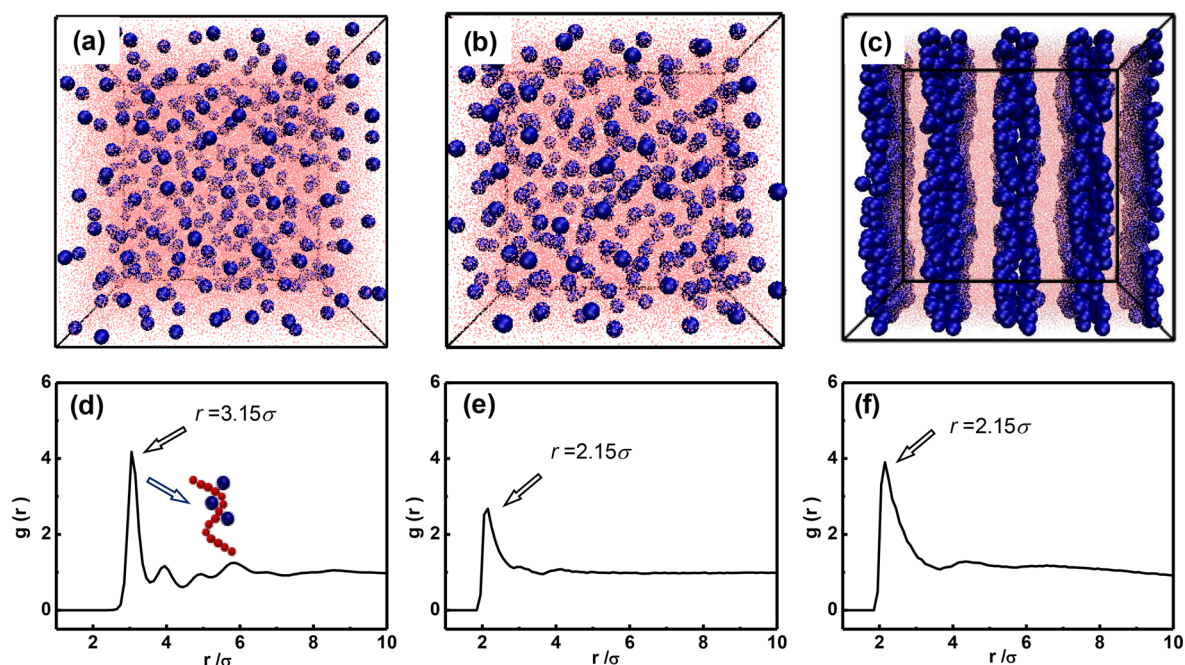
Figure 4. Equilibrium structures of $P_{24}N$-2 systems with (a) attractive, (b) neutral, and (c) repulsive NP−polymer interaction. Radial distribution functions between NPs for $P_{24}N$-2 in (d) attractive, (e) neutral, and (f) repulsive systems. The NP diameter and polymer chain length are set as $d = 2\sigma$ and $L = 24$, respectively. The blue and red colors in the structural snapshots are assigned to the NPs and polymer beads, respectively.

the values of $2.05 \times 10^{-4}\ \sigma^2/\tau$, $2.47 \times 10^{-4}\ \sigma^2/\tau$, and $3.82 \times 10^{-4}\ \sigma^2/\tau$, respectively. The D_{cm} and D_P for the P_{24} system are $2.21 \times 10^{-3}\ \sigma^2/\tau$ and $2.63 \times 10^{-3}\ \sigma^2/\tau$, respectively. Compared to the P_{24} system, both the D_{cm} and D_P of $P_{24}N$-2 system reduce by an order of magnitude. These data of diffusion coefficients suggest that the motions of whole chains and polymer segments are slowed down, which results in slower stress relaxation and enhanced dynamic moduli of NTPs. The curves of MSDs as a function of time for the NPs/polymer blend are also plotted and shown in Figure S2 of SI. The D_{cm}, D_N, and D_P of blend system are larger than those of $P_{24}N$-2 system. This suggests that NPs tethering with the end of polymers dramatically suppress the polymer motion.

The previous works about the viscoelasticity of NPs/polymer blend have demonstrated that the slowdown of polymer motion originates from the attractive NP−polymer interaction and the obstacles of NPs.[32,64] A salient feature of the NTPs is that the slowdown of polymer motion could also arise from the covalent bond connecting the NPs and the polymers. To examine the effect of this bond on the mobility of polymers, the MSDs of head and tail beads of polymer chains are calculated and shown in Figure 3c. The definitions of head and tail beads are shown in the inset of Figure 3c. It can be seen that the MSDs of head beads are much smaller than those of tail beads, suggesting that the introduction of covalent bond significantly suppresses the diffusion dynamics of head beads and then the suppression passes on to other beads. As a result, the motion of whole polymers slows down, leading to the enhancement of dynamic moduli. In Figure 3c, it is also demonstrated that the diffusion velocity of the head beads is larger than that of the NPs. The reason is that the head beads can not only transnationally move with the NPs, but also motion around the NP surfaces. In the following simulations, the other effects, (i.e., the attractive NP−polymer interaction and the obstacles of NPs) were also investigated by tuning the NP−polymer interaction and the molecular architecture.

3.2. Effect of NP−Polymer Interaction.

In this subsection, we focused on the effect of NP-polymer interaction on the viscoelasticity of NTPs. We considered three types of NP−polymer interaction, including attractive, repulsive, and neutral interactions. As mentioned above, the cutoff distance $r_{N−P}^c$ and the interaction strength $\varepsilon_{N−P}$ in the Lennard-Jones potential govern the NP−polymer interaction. The $r_{N−P}^c$ was set as a repulsive cutoff distance $2^{1/6}\sigma$ for the repulsive system and an attractive cutoff distance 2.5σ for the attractive system. To realize the neutral system, the $r_{N−P}^c$ was set as $1.4\ \sigma$ between the repulsive and attractive cutoff distances. The values of $\varepsilon_{N−P}$ for all of the systems were set as 5.0ε. The NP diameter and the polymer chain length were chosen as $d = 2\sigma$ and $L = 24$, respectively.

Figure 4 shows the equilibrium structures and the radial distribution functions $g(r)$ between NPs for the $P_{24}N$-2 systems with attractive, repulsive, and neutral NP−polymer interactions. The NPs uniformly disperse in the attractive and neutral systems, as shown in Figure 4a,b. In the attractive system, the $g(r)$ plot shows a pronounced peak at $r = 3.15\sigma$ and weak peaks at larger distance appear around $r = 4.0\sigma$, $r = 5.0\sigma$, and $r = 5.9\sigma$ (see Figure 4d), further verifying that the NPs are well separated by the polymers as schematically illustrated in the inset of Figure 4d. In the neutral system, however, the $g(r)$ plot shows a peak at $r = 2.15\sigma$ (see Figure 4e), indicating that a certain amount of NPs directly contact each other. This suggests that the dispersion degree of NPs in the attractive system is larger compared to that in the neutral system. In the repulsive system, the NPs form double-sheet structure and are separated by the polymer phase (see Figure 4c). The $g(r)$ plot shows a stronger peak at $r = 2.15\sigma$ (see Figure 4f) than that in the neutral system, suggesting that the dispersion degree of NPs is the smallest in the repulsive system.

The viscoelastic properties of $P_{24}N$-2 systems with attractive, repulsive, and neutral NP−polymer interactions were examined. G' and G'' as a function of shear frequency for these

systems are shown in Figure 5a. Both G' and G'' exhibit similar tendencies in response to the shear frequency for the attractive
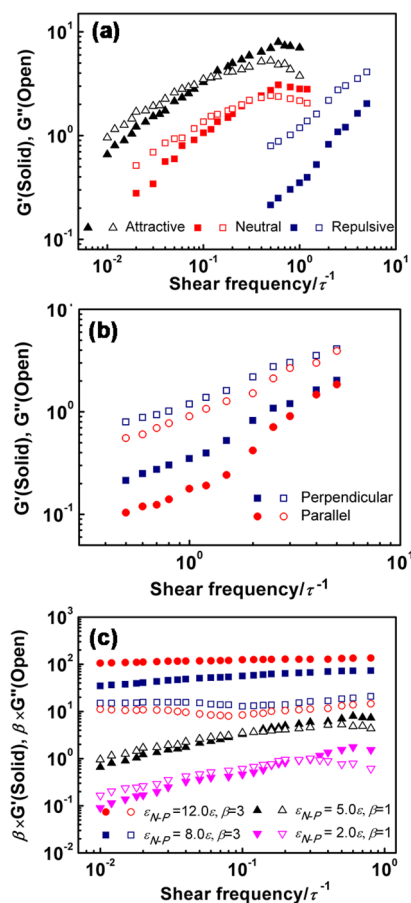

Figure 5. (a) Frequency sweeps of G' and G'' in the attractive, repulsive, and neutral systems. (b) Frequency sweeps of G' and G'' in the parallel shear and perpendicular shear of repulsive system. (c) Frequency sweeps of G' and G'' for the attractive systems with various ε_{N-P}. For clarity, the plots in (c) are shifted by factors β of 1, 1, 3, and 3 for the systems of $\varepsilon_{N-P} = 2.0\varepsilon$, $\varepsilon_{N-P} = 5.0\varepsilon$, $\varepsilon_{N-P} = 8.0\varepsilon$, and $\varepsilon_{N-P} = 12.0\varepsilon$, respectively.

and neutral systems, but the moduli in the attractive system are larger than those in the neutral system. This result verifies that the attractive NP-polymer interaction plays a role in the enhanced viscoelasticity of NTPs. The relaxation dynamics of polymers is slowed down by the attraction of NPs. One can also observe that G' and G'' in the repulsive system are much smaller than those in the other two systems, which arises from the relaxation of stress through the NPs aggregation.

It should be noted that the NTPs in the repulsive system form double-sheet structures with anisotropic characteristic and the shear direction is perpendicular to the sheets for calculating the G' and G'' in Figure 5a. The G' and G'' are also calculated by shearing in the direction parallel to the sheets and the results are shown in Figure 5b. It can be seen that G' and G'' calculated by the parallel shear are smaller than those calculated by the perpendicular shear. The reason is that the length scale of NP sheets in the parallel direction is larger than that in the perpendicular direction; therefore, the stress can relax even faster through the NP sheets in the parallel shear. In the attractive and neutral systems, however, the structures of NTPs are isotropic, and thus the dynamic moduli calculated by

shearing in all the three orthogonal directions are close to each other (not shown).

Since the attractive system exhibits distinct viscoelasticity, the effect of NP−polymer interaction strength on the viscoelasticity in the attractive system was further explored. The curves of G' and G'' versus shear frequency for various interaction strengths ε_{N-P} are shown in Figure 5c. For clarity, the plots are shifted vertically, and the shift factors β are equal to 1, 1, 3, and 3 for the systems with $\varepsilon_{N-P} = 2.0\varepsilon$, $\varepsilon_{N-P} = 5.0\varepsilon$, $\varepsilon_{N-P} = 8.0\varepsilon$, and $\varepsilon_{N-P} = 12.0\varepsilon$, respectively. Figure 5c shows that both G' and G'' increase with increasing ε_{N-P}. For the systems of $\varepsilon_{N-P} = 8.0\varepsilon$ and $\varepsilon_{N-P} = 12.0\varepsilon$, G' is significantly larger than G'', indicating that these NTPs exhibit solid-like viscoelastic characteristics. This behavior is different from that in the systems of $\varepsilon_{N-P} = 2.0\varepsilon$ and $\varepsilon_{N-P} = 5.0\varepsilon$, where a liquid-to-solid transition takes place near $\omega = 0.1\tau^{-1}$. Compared to the system of $\varepsilon_{N-P} = 5.0\varepsilon$, the transition point in the system of $\varepsilon_{N-P} = 2.0\varepsilon$ shifts to a larger frequency and the values of G' and G'' are smaller. The absence of liquid-to-solid transition in systems of $\varepsilon_{N-P} = 8.0\varepsilon$ and $\varepsilon_{N-P} = 12.0\varepsilon$ attributes to the fact that the transition points are shifted to a lower frequency out of measured range.

Figure 6 shows the MSDs of polymer beads and center-of-mass of polymers as a function of time in the attractive system
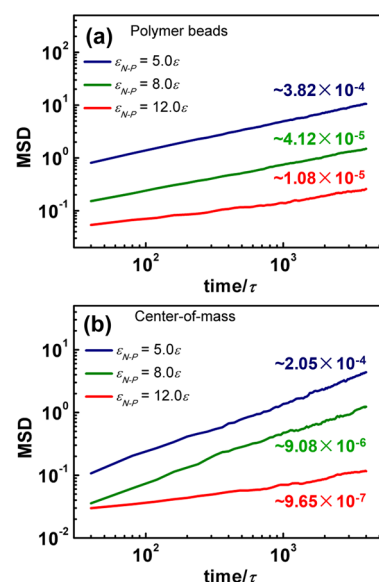

Figure 6. MSDs of (a) polymer beads and (b) center-of-mass of polymers as a function of simulation time for the $P_{24}N$-2 systems with various NP−polymer interaction strengths of $\varepsilon_{N-P} = 5.0\varepsilon$, $\varepsilon_{N-P} = 8.0\varepsilon$, and $\varepsilon_{N-P} = 12.0\varepsilon$. The diffusion coefficients are highlighted in the plots.

with various strengths of NP−polymer interaction. One can deduce that the D_P decreases significantly from $3.82 \times 10^{-4}\ \sigma^2/\tau$ to $4.12 \times 10^{-5}\ \sigma^2/\tau$ as ε_{N-P} increases from 5.0ε to 8.0ε. It even drops to $1.08 \times 10^{-5}\ \sigma^2/\tau$ in the system with $\varepsilon_{N-P} = 12.0\varepsilon$. These further verify that the attractive NP−polymer interaction suppresses the motion of polymer beads. A similar tendency is observed for D_{cm} with increasing ε_{N-P} (i.e., the values of D_{cm} are $2.05 \times 10^{-4}\ \sigma^2/\tau$, $9.08 \times 10^{-6}\ \sigma^2/\tau$, and $9.65 \times 10^{-7}\ \sigma^2/\tau$ for the systems of $\varepsilon_{N-P} = 5.0\varepsilon$, $\varepsilon_{N-P} = 8.0\varepsilon$, and $\varepsilon_{N-P} = 12.0\varepsilon$, respectively). One can also deduce that the increase of ε_{N-P} has more marked effect on the D_{cm} than that on the D_P, suggesting that the motion of whole chains can be suppressed more prominently than that of polymer beads. These behaviors

originate from the fact that the motion of a polymer chain is frustrated near the NP surface where the polymer beads could not pass through.

3.3. Effects of Molecular Architectures. As illustrated above, tethering NPs with polymers suppresses the polymer motions and enhances the dynamic moduli. We then constructed NTPs with various molecular architecture parameters, such as the NP diameter d and the polymer chain length L, to examine how these parameters affect their viscoelasticity. In the simulations, the NTP volume fraction ϕ_{NTP} is invariable and the volume of the initial box is fixed at $22.7 \times 22.7 \times 22.7\sigma^3$, hence, the number of NTPs is tuned. The cutoff distance and interaction strength of NP-polymer interaction are set as 2.5σ and 5.0ε, respectively.

Three types of NTPs with $d = 2\sigma$, $d = 3\sigma$, and $d = 4\sigma$ (denoted by $P_{24}N$-2, $P_{24}N$-3, and $P_{24}N$-4, respectively) are constructed, and the frequency sweeps of G' and G'' for these NTPs are shown in Figure 7a. Both G' and G'' of the $P_{24}N$-3
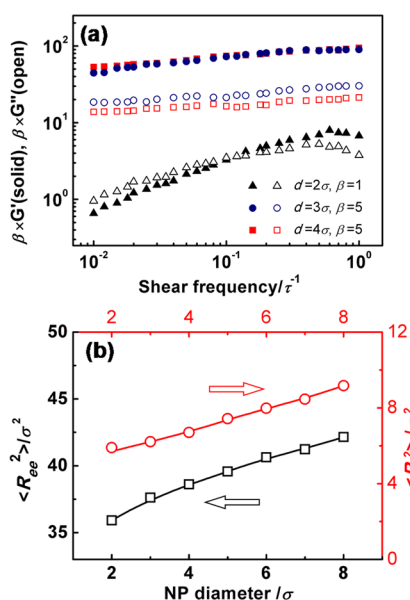

Figure 7. (a) G' and G'' as a function of shear frequency for the $P_{24}N$-d systems with NP diameters $d = 2\sigma$, $d = 3\sigma$, and $d = 4\sigma$. The plots are shifted by the factors β of 1, 5, and 5 for the systems of $d = 2\sigma$, $d = 3\sigma$, and $d = 4\sigma$, respectively. (b) The mean square end-to-end distance $\langle R_{ee}^2 \rangle$ and the mean square radius of gyration $\langle R_g^2 \rangle$ as a function of NP diameter. The ε_{N-P} and the r_{NP}^c have values of 5.0ε and 2.5σ, respectively.

and $P_{24}N$-4 systems are larger than those of the $P_{24}N$-2 system, indicating that increasing the NP diameter d can also enhance the dynamic moduli. From the curves of MSDs versus time (see Figure S3a,b of SI), one can see that the polymer dynamics is suppressed dramatically as d increases. To get insight into the microscopic origin of slowdown of polymer dynamics, the mean square end-to-end distance $\langle R_{ee}^2 \rangle$ and the mean square radius of gyration $\langle R_g^2 \rangle$ of polymers in these systems were calculated and shown in Figure 7b. As proposed by Kremer, the mean square end-to-end distance of polymers is $\langle R_{ee}^2 \rangle = l^2 l_p^2 (L-1)$,[62] where l is the average bond length and l_p is the persistence length. As shown in Figure 7b, the $\langle R_{ee}^2 \rangle$ and $\langle R_g^2 \rangle$ increase with increasing d, thereby the persistence length l_p increases because both l and L are invariable. On the one hand, the polymers become stiffer (i.e., the l_p increases) with increasing

NP diameter, which arises from the loss of conformational entropy caused by the obstacle of NPs. On the other hand, the polymers have to drag heavier NPs as the NP diameter increases. These two factors lead to the slowdown of polymer dynamics.

The viscoelasticity of NTPs with various polymer chain lengths was also examined. The curves of G' and G'' as a function of shear frequency ω for three samples of $P_{16}N$-2, $P_{24}N$-2, and $P_{32}N$-2 are shown in Figure 8a. The $P_{16}N$-2 system
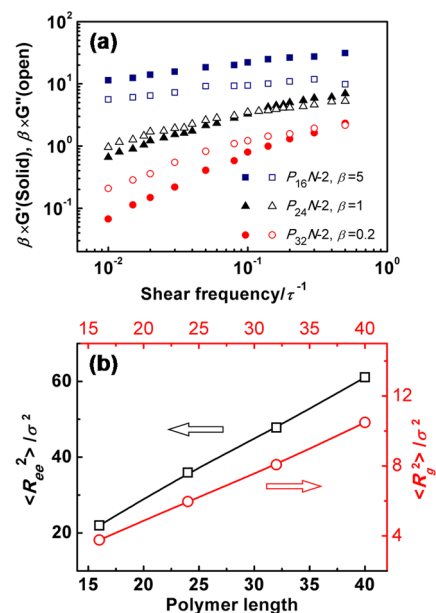

Figure 8. (a) G' and G'' as a function of shear frequency for the NPs-tethering polymers with various chain lengths L. The NP diameter is fixed at $d = 2\sigma$. The plots are shifted by the factors β of 5, 1, and 0.2 for the systems of $P_{16}N$-2, $P_{24}N$-2, and $P_{32}N$-2, respectively. (b) $\langle R_{ee}^2 \rangle$ and $\langle R_g^2 \rangle$ as a function of polymer chain length. The ε_{N-P} and the r_{NP}^c are set as 5.0ε and 2.5σ, respectively.

exhibits solid-like viscoelasticity (i.e., $G' > G''$ in the measured range). The $P_{24}N$-2 and $P_{32}N$-2 systems show liquid-to-solid transition with increasing ω, and the transition point shifts to a higher frequency for the $P_{32}N$-2 system compared to that for the $P_{24}N$-2 system. Additionally, both G' and G'' decrease with increasing L, which could arise from the decrease of size ratio of NPs to polymers. To characterize the polymer size, the $\langle R_{ee}^2 \rangle$ and $\langle R_g^2 \rangle$ of polymers were calculated and shown in Figure 8b. Both the $\langle R_{ee}^2 \rangle$ and $\langle R_g^2 \rangle$ increase linearly with increasing L, and thus the persistence length l_p maintains invariable according to the relationship of $\langle R_{ee}^2 \rangle = l^2 l_p^2 (L-1)$. This suggests that the conformation of polymers is unaffected by increasing the polymer chain length. For the $P_{16}N$-2 system, the polymer size is smaller than the NP size (i.e., $R_g/d < 1$, see Figure 8b), and thus, the mobility of polymers is suppressed significantly because the polymers have to drag heavy NPs. On the contrary, for the $P_{24}N$-2 and $P_{32}N$-2 systems, the polymer size is larger than the NP size (i.e., $R_g/d > 1$, see Figure 8b), and thus, the suppression of polymer motions is weaker than that in $P_{16}N$-2 system. This is further verified in the MSD curves (Figure S3c,d of SI) that the MSDs increase by an order of magnitude, as the polymer chain length increases from 16 to 24.

From the observations of Figures 7 and 8, it is implied that the ratio of the NP size to the polymer size could play a role in

the viscoelasticity. To evaluate the role of NP size, we conducted a series of NEMD simulations for the NTPs with similar NP volume fraction ϕ_N, which is defined as the ratio of NP volume to the sum of NP and polymer bead volume. Herein, we fix the ϕ_N at 0.5 (e.g., P_8N-2 and $P_{24}N$-3). The frequency sweeps of G' and G'' for the P_8N-2 and $P_{24}N$-3 systems are shown in Figure S4 of SI. It can be seen that the moduli of P_8N-2 system are close to those of $P_{24}N$-3 system. This suggests that the mechanical properties of different systems are similar when the values of ϕ_N are close. Despite the similarity, it will be devoted to thoroughly elucidating the generality of viscoelasticity of NTPs in terms of the nanoparticle volume fraction in further work.

3.4. Comparison with Experimental Observations.

This study has shown that the dynamic moduli are enhanced in the NTPs compared to the homopolymers (see Figure 2b) and bare NPs/polymer blends with the same polymer chain length and NP diameter (see Figure S1a). Some experimental observations in the literatures are available, supporting our theoretical results. For instance, Genix and coauthors studied the linear rheology of silica NPs tethering styrene butadiene rubber (SBR).[26] They found that the characteristic relaxation time and the dynamic moduli gradually increase with increasing the tethering density of silica NPs. Archer's group investigated the dynamics of SiO_2-tethered-*cis*-1,4-polyisoprene.[65] They found that the tethered systems can enhance the dynamic moduli compared to the untethered system. These experimental results are consistent with our theoretical results (i.e., the NTPs show enhanced dynamic moduli and slower polymer dynamics compared to the bare NPs/polymer blend).

Additionally, our simulation results confirm the experimental observations that the dynamic moduli of systems with well dispersed NPs are higher than those of systems with aggregated NPs structures (see Figures 4a−c and 5a). Liu et al. studied the structure-dynamic relationships in the composites of PS-grafted iron oxide using X-ray photon correlation spectroscopy.[28] The characteristic relaxation of polymers reduces dramatically with decreasing the dispersion degree of NPs, which is confirmed by our results of Figure 5a. Our simulation results also reveal that the molecular architectures, such as the NP diameter and the polymer chain length can tune the viscoelasticity. It was found that increasing the ratio of the NP diameter to the polymer chain length can enhance the dynamic moduli. This result is in accordance with some experimental results. For example, Archer's group also observed that increasing the molecular weight of tethered polymer speeds up chain relaxation dynamics and reduces dynamic moduli.[65]

Beyond the reproductions of general features of experimental findings for the NTPs, the simulations can reveal the physical origin of viscoelastic properties of polymeric systems and deepen the understanding of experimental observations. This is a practical signification for experimentally designing and fabricating advanced materials. In the simulations, it is convenient to visualize the morphology and to obtain the molecular information. For instance, the dispersion state of NPs in the polymer phase can be easily characterized by the radial distribution function $g(r)$ between NPs (see Figure 4d−f). The NPs in the system of attractive NP−polymer interaction are well dispersed as reflected by the pronounced peak appearing at $r = 3.15\sigma$ in the $g(r)$ curves, while they are aggregated in the repulsive system as the peak appears at $r = 2.15\sigma$. Moreover, it is facile to calculate the dynamic parameters which can reveal the microscopic origin of enhanced

viscoelasticity in the attractive system. For example, the diffusion dynamics of NTPs can be easily elucidated by the MSDs of NPs, polymer beads, and center-of-mass of polymer chains. The diffusion coefficients of these motion units in the attractive system increase compared to those of the homopolymer (see Figure 3), and the increase of diffusion coefficients gets more significant as the strength of the NP−polymer interaction increases (see Figure 6).

4. CONCLUSIONS

We applied the nonequilibrium molecular dynamics simulations to study the viscoelasticity of NPs-tethering polymers. The results show that the storage and loss moduli can be enhanced in the NPs-tethering polymers, compared to those in the homopolymers or bare NPs/polymer blends. From the physical origin, the enhancement of dynamic moduli originates from the slowdown of the dynamics of both the whole polymers and the segments. The slowdown of polymer dynamics arises from (1) the attractive NP−polymer interaction, (2) the covalent bond between the NPs and the polymer chains, and (3) the obstacle of NPs. In addition, the effect of molecular architectures, such as the NP diameter and the polymer chain length on the viscoelasticity of NPs-tethering polymers were examined. It was found that increasing the NP diameter or decreasing the polymer chain length can enhance the dynamic moduli. Our research revealed the physical origin of distinct viscoelasticity of NPs-tethering polymers and could provide useful information for preparing advanced materials based on the organic/inorganic hybrid strategy.

■ ASSOCIATED CONTENT

ⓢ Supporting Information

The Supporting Information is available free of charge on the ACS Publications website at DOI: 10.1021/acs.jpcc.7b10455.

> Comparison to the NPs/polymer blend, the temporal evolutions of MSDs, and the viscoelasticity of NP-tethering polymers with similar NP volume fraction (PDF).

■ AUTHOR INFORMATION

Corresponding Authors

*E-mail: jlin@ecust.edu.cn.
*E-mail: zhangls@ecust.edu.cn. Phone: +86-21-6425-1615.

ORCID ⓘ

Pengxiang Xu: 0000-0001-5411-9566
Jiaping Lin: 0000-0001-9633-4483
Liangshun Zhang: 0000-0002-0182-7486

Notes

The authors declare no competing financial interest.

■ REFERENCES

(1) Glotzer, S. C. Some Assembly Required. *Science* 2004, *306*, 419−420.

(2) Iacovella, C. R.; Keys, A. S.; Horsch, M. A.; Glotzer, S. C. Icosahedral Packing of Polymer-Tethered Nanospheres and Stabilization of the Gyroid Phase. *Phys. Rev. E* **2007**, *75*, 040801.

(3) Moll, J. F.; Akcora, P.; Rungta, A.; Gong, S.; Colby, R. H.; Benicewicz, B. C.; Kumar, S. K. Mechanical Reinforcement in Polymer Melts Filled with Polymer Grafted Nanoparticles. *Macromolecules* **2011**, *44*, 7473−7477.

(4) Tao, P.; Viswanath, A.; Schadler, L. S.; Benicewicz, B. C.; Siegel, R. W. Preparation and Optical Properties of Indium Tin Oxide/Epoxy Nanocomposites with Polyglycidyl Methacrylate Grafted Nanoparticles. *ACS Appl. Mater. Interfaces* **2011**, *3*, 3638−3645.

(5) Sanchez, C.; Belleville, P.; Popall, M.; Nicole, L. Applications of Advanced Hybrid Organic-Inorganic Nanomaterials: from Laboratory to Market. *Chem. Soc. Rev.* **2011**, *40*, 696−753.

(6) Kumar, S. K.; Jouault, N.; Benicewicz, B.; Neely, T. Nanocomposites with Polymer Grafted Nanoparticles. *Macromolecules* **2013**, *46*, 3199−3214.

(7) Aricò, A. S.; Bruce, P.; Scrosati, B.; Tarascon, J. M.; van Schalkwijk, W. Nanostructured Materials for Advanced Energy Conversion and Storage Devices. *Nat. Mater.* **2005**, *4*, 366−377.

(8) Akcora, P.; Kumar, S. K.; Sakai, V. G.; Li, Y.; Benicewicz, B. C.; Schadler, L. S. Segmental Dynamics in PMMA-Grafted Nanoparticle Composites. *Macromolecules* **2010**, *43*, 8275−8281.

(9) Srivastava, S.; Agarwal, P.; Archer, L. A. Tethered Nanoparticle-Polymer Composites: Phase Stability and Curvature. *Langmuir* **2012**, *28*, 6276−6281.

(10) Xu, C.; Ohno, K.; Ladmiral, V.; Composto, R. J. Dispersion of Polymer-Grafted Magnetic Nanoparticles in Homopolymers and Block Copolymers. *Polymer* **2008**, *49*, 3568−3577.

(11) Smith, G. D.; Bedrov, D. Dispersing Nanoparticles in a Polymer Matrix: Are Long, Dense Polymer Tethers Really Necessary? *Langmuir* **2009**, *25*, 11239−11243.

(12) Lim, J.; zur Borg, L.; Dolezel, S.; Schmid, F.; Char, K.; Zentel, R. Strategy for Good Dispersion of Well-Defined Tetrapods in Semiconducting Polymer Matrices. *Macromol. Rapid Commun.* **2014**, *35*, 1685−1691.

(13) Kawauchi, T.; Kumaki, J.; Yashima, E. Synthesis, Isolation via Self-Assembly, and Single-Molecule Observation of a [60]Fullerene-End-Capped Isotactic Poly(methyl methacrylate). *J. Am. Chem. Soc.* **2005**, *127*, 9950−9951.

(14) Chevigny, C.; Dalmas, F.; Di Cola, E.; Gigmes, D.; Bertin, D.; Boué, F.; Jestin, J. Polymer-Grafted-Nanoparticles Nanocomposites: Dispersion, Grafted Chain Conformation, and Rheological Behavior. *Macromolecules* **2011**, *44*, 122−133.

(15) Sunday, D. F.; Green, D. L. Thermal and Rheological Behavior of Polymer Grafted Nanoparticles. *Macromolecules* **2015**, *48*, 8651−8659.

(16) Senses, E.; Jiao, Y.; Akcora, P. Modulating Interfacial Attraction of Polymer-Grafted Nanoparticles in Melts under Shear. *Soft Matter* **2014**, *10*, 4464−4470.

(17) Wang, X.-M.; Shao, Y.; Xu, J.; Jin, X.; Shen, R.-H.; Jin, P.-F.; Shen, D.-W.; Wang, J.; Li, W.; He, J.; Ni, P.; Zhang, W.-B. Precision Synthesis and Distinct Assembly of Double-Chain Giant Surfactant Regioisomers. *Macromolecules* **2017**, *50*, 3943−3953.

(18) Yue, K.; Liu, C.; Huang, M.; Huang, J.; Zhou, Z.; Wu, K.; Liu, H.; Lin, Z.; Shi, A.-C.; Zhang, W.-B.; Cheng, S. Z. D. Self-Assembled Structures of Giant Surfactants Exhibit a Remarkable Sensitivity on Chemical Compositions and Topologies for Tailoring Sub-10 nm Nanostructures. *Macromolecules* **2017**, *50*, 303−314.

(19) Lin, Z.; Sun, J.; Zhou, Y.; Wang, Y.; Xu, H.; Yang, X.; Su, H.; Cui, H.; Aida, T.; Zhang, W.; Cheng, S. Z. D. A Noncrystallization Approach toward Uniform Thylakoids-like 2D ″Nano-coins″ and Their Grana-like 3D Suprastructures. *J. Am. Chem. Soc.* **2017**, *139*, 5883−5889.

(20) Iacovella, C. R.; Horsch, M. A.; Zhang, Z.; Glotzer, S. C. Phase Diagrams of Self-Assembled Mono-Tethered Nanospheres from Molecular Simulation and Comparison to Surfactants. *Langmuir* **2005**, *21*, 9488−9494.

(21) Zhu, X.; Wang, L.; Lin, J.; Zhang, L. Ordered Nanostructures Self-Assembled from Block Copolymer Tethered Nanoparticles. *ACS Nano* **2010**, *4*, 4979−4988.

(22) Lafitte, T.; Kumar, S. K.; Panagiotopoulos, A. Z. Self-Assembly of Polymer-Grafted Nanoparticles in Thin Films. *Soft Matter* **2014**, *10*, 786−794.

(23) Zhang, B.; Edwards, B. J. The Effect of Particle Size on the Morphology and Thermodynamics of Diblock Copolymer/Tethered-Particle Membranes. *J. Chem. Phys.* **2015**, *142*, 214907.

(24) Zhao, D.; Di Nicola, M.; Khani, M. M.; Jestin, J.; Benicewicz, B. C.; Kumar, S. K. Self-Assembly of Monodisperse versus Bidisperse Polymer-Grafted Nanoparticles. *ACS Macro Lett.* **2016**, *5*, 790−795.

(25) Zhang, T.; Fu, C.; Yang, Y.; Qiu, F. Extremely Asymmetric Phase Diagram of Homopolymer-Monotethered Nanoparticles: Competition between Chain Conformational Entropy and Particle Steric Interaction. *J. Chem. Phys.* **2017**, *146*, 054902.

(26) Baeza, G. P.; Genix, A.-C.; Degrandcourt, C.; Petitjean, L.; Gummel, J.; Schweins, R.; Couty, M.; Oberdisse, J. Effect of Grafting on Rheology and Structure of a Simplified Industrial Nanocomposite Silica/SBR. *Macromolecules* **2013**, *46*, 6621−6633.

(27) Moll, J.; Kumar, S. K.; Snijkers, F.; Vlassopoulos, D.; Rungta, A.; Benicewicz, B. C.; Gomez, E.; Ilavsky, J.; Colby, R. H. Dispersing Grafted Nanoparticle Assemblies into Polymer Melts through Flow Fields. *ACS Macro Lett.* **2013**, *2*, 1051−1055.

(28) Liu, S.; Senses, E.; Jiao, Y.; Narayanan, S.; Akcora, P. Structure and Entanglement Factors on Dynamics of Polymer-Grafted Nanoparticles. *ACS Macro Lett.* **2016**, *5*, 569−573.

(29) McEwan, M.; Green, D. Rheological Impacts of Particle Softness on Wetted Polymer-Grafted Silica Nanoparticles in Polymer Melts. *Soft Matter* **2009**, *5*, 1705−1716.

(30) Maillard, D.; Kumar, S. K.; Fragneaud, B.; Kysar, J. W.; Rungta, A.; Benicewicz, B. C.; Deng, H.; Brinson, L. C.; Douglas, J. F. Mechanical Properties of Thin Glassy Polymer Films Filled with Spherical Polymer-Grafted Nanoparticles. *Nano Lett.* **2012**, *12*, 3909−3914.

(31) Srivastava, S.; Shin, J. H.; Archer, L. A. Structure and Rheology of Nanoparticle−Polymer Suspensions. *Soft Matter* **2012**, *8*, 4097−4108.

(32) Pryamitsyn, V.; Ganesan, V. Origins of Linear Viscoelastic Behavior of Polymer-Nanoparticle Composites. *Macromolecules* **2006**, *39*, 844−856.

(33) Ma, S.; Hu, Y.; Wang, R. Self-Assembly of Polymer Tethered Molecular Nanoparticle Shape Amphiphiles in Selective Solvents. *Macromolecules* **2015**, *48*, 3112−3120.

(34) Jayaraman, A.; Schweizer, K. S. Structure and Assembly of Dense Solutions and Melts of Single Tethered Nanoparticles. *J. Chem. Phys.* **2008**, *128*, 164904.

(35) Starr, F. W.; Douglas, J. F.; Glotzer, S. C. Origin of Particle Clustering in a Simulated Polymer Nanocomposite and Its Impact on Rheology. *J. Chem. Phys.* **2003**, *119*, 1777−1788.

(36) Chen, Y.; Liu, L.; Yang, Q.; Wen, S.; Zhang, L.; Zhong, C. Computational Study of Nanoparticle Dispersion and Spatial Distribution in Polymer Matrix under Oscillatory Shear Flow. *Langmuir* **2013**, *29*, 13932−13942.

(37) Shen, J.; Liu, J.; Li, H.; Gao, Y.; Li, X.; Wu, Y.; Zhang, L. Molecular Dynamics Simulations of the Structural, Mechanical and Visco-elastic Properties of Polymer Nanocomposites Filled with Grafted Nanoparticles. *Phys. Chem. Chem. Phys.* **2015**, *17*, 7196−7207.

(38) Hattemer, G. D.; Arya, G. Viscoelastic Properties of Polymer-Grafted Nanoparticle Composites from Molecular Dynamics simulations. *Macromolecules* **2015**, *48*, 1240−1255.

(39) Tang, T.-Y.; Arya, G. Anisotropic Three-Particle Interactions between Spherical Polymer-Grafted Nanoparticles in a Polymer Matrix. *Macromolecules* **2017**, *50*, 1167−1183.

(40) Xu, Z.; Lin, J.; Zhang, Q.; Wang, L.; Tian, X. Theoretical Simulations of Nanostructures Self-assembled from Copolymer Systems. *Polym. Chem.* **2016**, *7*, 3783−3811.

(41) Maurel, G.; Goujon, F.; Schnell, B.; Malfreyt, P. Multiscale Modeling of the Polymer−Silica Surface Interaction: From Atomistic to Mesoscopic Simulations. *J. Phys. Chem. C* **2015**, *119*, 4817−4826.

(42) Gavrilov, A. A.; Chertovich, A. V.; Khalatur, P. G.; Khokhlov, A. R. Study of the Mechanisms of Filler Reinforcement in Elastomer Nanocomposites. *Macromolecules* **2014**, *47*, 5400−5408.

(43) Ghanbari, A.; Rahimi, M.; Dehghany, J. Influence of Surface Grafted Polymers on the Polymer Dynamics in a Silica−Polystyrene Nanocomposite: A Coarse-Grained Molecular Dynamics Investigation. *J. Phys. Chem. C* **2013**, *117*, 25069−25076.

(44) Li, Y.; Kröger, M.; Liu, W. K. Dynamic Structure of Unentangled Polymer Chains in the Vicinity of Non-Attractive Nanoparticles. *Soft Matter* **2014**, *10*, 1723−1737.

(45) Li, Y.; Kröger, M.; Liu, W. K. Nanoparticle Effect on the Dynamics of Polymer Chains and Their Entanglement Network. *Phys. Rev. Lett.* **2012**, *109*, 118001.

(46) Goyal, S.; Escobedo, F. A. Structure and Transport Properties of Polymer Grafted Nanoparticles. *J. Chem. Phys.* **2011**, *135*, 184902.

(47) Chen, Y.; Li, Z.; Wen, S.; Yang, Q.; Zhang, L.; Zhong, C.; Liu, L. Molecular Simulation Study of Role of Polymer-Particle Interactions in the Strain-Dependent Viscoelasticity of Elastomers (Payne Effect). *J. Chem. Phys.* **2014**, *141*, 104901.

(48) Jiang, T.; Wang, L.; Lin, J. Distinct Mechanical Properties of Nanoparticle-Tethering Polymers. *RSC Adv.* **2014**, *4*, 35272−35283.

(49) Dupuy, L. M.; Tadmor, E. B.; Miller, R. E.; Phillips, R. Finite-Temperature Quasicontinuum: Molecular Dynamics without All the Atoms. *Phys. Rev. Lett.* **2005**, *95*, 060202.

(50) Wang, Q.; Keffer, D. J.; Nicholson, D. M.; Thomas, J. B. Coarse-Grained Molecular Dynamics Simulation of Polyethylene Terephthalate (PET). *Macromolecules* **2010**, *43*, 10722−10734.

(51) Piserchia, A.; Zerbetto, M.; Salvia, M.-V.; Salassa, G.; Gabrielli, L.; Mancin, F.; Rastrelli, F.; Frezzato, D. Conformational Mobility in Monolayer-Protected Nanoparticles: From Torsional Free Energy Profiles to NMR Relaxation. *J. Phys. Chem. C* **2015**, *119*, 20100−20110.

(52) Liu, J.; Cao, D.; Zhang, L. Molecular Dynamics Study on Nanoparticle Diffusion in Polymer Melts: A Test of the Stokes-Einstein Law. *J. Phys. Chem. C* **2008**, *112*, 6653−6661.

(53) Liu, J.; Wu, S.; Zhang, L.; Wang, W.; Cao, D. Molecular Dynamics Simulation for insight into Microscopic Mechanism of Polymer Reinforcement. *Phys. Chem. Chem. Phys.* **2011**, *13*, 518−529.

(54) Allen, M. P.; Tildesley, D. J. *Computer Simulation of Liquids*; Oxford University: New York, 1987.

(55) Soddemann, T.; Dünweg, B.; Kremer, K. Dissipative Particle Dynamics: a Useful Thermostat for Equilibrium and Nonequilibrium Molecular Dynamics Simulations. *Phys. Rev. E: Stat. Phys., Plasmas, Fluids, Relat. Interdiscip. Top.* **2003**, *68*, 046702.

(56) Jung, G.; Schmid, F. Computing Bulk and Shear Viscosities from Simulations of Fluids with Dissipative and Stochastic Interactions. *J. Chem. Phys.* **2016**, *144*, 204104.

(57) Xu, P.; Lin, J.; Wang, L.; Zhang, L. Shear Flow Behaviors of Rod-Coil Diblock Copolymers in Solution: A Nonequilibrium Dissipative Particle Dynamics Simulation. *J. Chem. Phys.* **2017**, *146*, 184903.

(58) Plimpton, S. Fast Parallel Algorithms for Short-Range Molecular Dynamics. *J. Comput. Phys.* **1995**, *117*, 1−19.

(59) Payne, A. R. The Dynamic Properties of Carbon Black-Loaded Natural Rubber Vulcanizates. Part I. *J. Appl. Polym. Sci.* **1962**, *6*, 57−63.

(60) Gan, S.; Wu, Z. L.; Xu, H.; Song, Y.; Zheng, Q. Viscoelastic Behaviors of Carbon Black Gel Extracted from Highly Filled Natural Rubber Compounds: Insights into the Payne Effect. *Macromolecules* **2016**, *49*, 1454−1463.

(61) Raos, G.; Casalegno, M. Nonequilibrium Simulations of Filled Polymer Networks: Searching for the Origins of Reinforcement and Nonlinearity. *J. Chem. Phys.* **2011**, *134*, 054902.

(62) Kremer, K.; Grest, G. S. Dynamics of Entangled Linear Polymer Melts: A Molecular Dynamics Simulation. *J. Chem. Phys.* **1990**, *92*, 5057−5086.

(63) Li, Y. W.; Zhu, Y. L.; Sun, Z. Y. Decoupling of Relaxation and Diffusion in Random Pinning Glass-forming Liquids. *J. Chem. Phys.* **2015**, *142*, 124507.

(64) Lin, Y.; Liu, L.; Xu, G.; Zhang, D.; Guan, A.; Wu, G. Interfacial Interactions and Segmental Dynamics of Poly(vinyl acetate)/Silica Nanocomposites. *J. Phys. Chem. C* **2015**, *119*, 12956−12966.

(65) Kim, S. A.; Mangal, R.; Archer, L. A. Relaxation Dynamics of Nanoparticle-Tethered Polymer Chains. *Macromolecules* **2015**, *48*, 6280−6293.